ANALYSIS OF VTVL AND VTHL REUSABLE LAUNCH VEHICLE CONFIGURATIONS

Conference Paper · January 2019

CITATION
1

READS
220

7 authors, including:

Sven Stappert
Polaris Raumflugzeuge
81 PUBLICATIONS **460** CITATIONS
SEE PROFILE

Jascha Wilken
German Aerospace Center (DLR)
50 PUBLICATIONS **261** CITATIONS
SEE PROFILE

Christian Hantz
German Aerospace Center (DLR)
12 PUBLICATIONS **53** CITATIONS
SEE PROFILE

ANALYSIS OF VTVL AND VTHL REUSABLE LAUNCH VEHICLE CONFIGURATIONS

Leonid Bussler, Sven Stappert, Jascha Wilken, Martin Sippel, Ingrid Dietlein
DLR Institute of Space Systems, SART, Bremen, Germany, Leonid.Bussler@dlr.de
Sebastian Karl
DLR Institute of Aerodynamics and Flow Technology, Goettingen, Germany, Sebastian.Karl@dlr.de
Christian Hantz
DLR Institute of Aerodynamics and Flow Technology, Cologne, Germany, Christian.Hantz@dlr.de

ABSTRACT

The German Aerospace Centre (DLR) is conducting systematic analyses of reusable space transportation configurations. Two-stage vertical take-off vertical landing (VTVL) and winged, vertical take-off horizontal landing (VTHL) partially reusable launcher configurations are systematically analyzed. The investigated configurations consider reusable first stages that either perform a return to launch site or land down range of the launch site. The propellant combinations analyzed include LOX/LH2, LOX/LCH4 and LOX/RP-1. Staged combustion and gas generator cycle engines are taken into account. The same type of engines with different expansion ratios are used on the reusable first stages and the expendable upper stages. Major analysis objectives are the comparison of various reusable launch vehicle configurations under similar design assumptions as well as the identification of their critical aspects, benefits and drawbacks.

Index Terms — Reusable Launch Vehicles, VTVL, VTHL

Acronyms

AoA	Angle Of Attack
DRL	Down Range Landing
FB	Fly-Back
GG	Gas Generator
GLOM	Gross Lift-Off Mass
IAC	In-Air-Capturing
LCH4	Liquid Methane
LH2	Liquid Hydrogen
LOX	Liquid Oxygen
P/L	Payload
RANS	Reynolds-Averaged Navier-Stokes
RP-1	Rocket Propellant 1 (Kerosene)
SART	Space Launcher Systems Analysis
SC	Staged Combustion
SES	Société Européenne des Satellites
VTHL	Vertical Take-Off Horizontal Landing
VTVL	Vertical Take-Off Vertical Landing

Nomenclature

Isp	Specific Impulse	[s]
L/D	Lift-to-drag ratio	[-]
T/W	Thrust-to-weight ratio	[-]
ΔV	Delta velocity	[km/s]

1. INTRODUCTION

The presented work is part of a general, systematic analysis of reusable launch vehicles (RLV) in DLR, [1] - [3]. This investigation is motivated by an aspiration to identify suitable and advantageous concept designs for a future European reusable launch system. Prior to any reuse the stage has to be recovered. This necessity poses the question of how to recover those parts that shall be re-used, which recovery strategy is most advantageous and what are the technologies to be developed. For this purpose DLR has committed a large system study comparing numerous Two-Stage-To-Orbit (TSTO) concepts containing reusable first stages with a specific focus on comparing various recovery strategies for the first stage. Special emphasis is placed on defining similar design assumptions for this comparison. Considered recovery approaches involve strategies based on horizontal landing of a winged stage and strategies based on vertical landing. The winged fly-back boosters perform an unpowered atmospheric reentry after separating from the upper stage and return to launch site performing a powered, subsonic cruise flight with on-board air-breathing engines. The so called In-Air-Capturing method attempts to achieve smaller and lighter reusable stages by towing the winged stages back to launch site by means of an aircraft, [4]. In contrast to winged stages, vertical landing concepts rely on rocket engines for decelerating and landing the reusable first stage.

During the first phase of this study, a larger number of both VTVL as well as VTHL configurations is analyzed and predesigned. Different fuel types as well as different engine cycles have been part of the design space during this study phase. In a second step VTVL and VTHL configurations are selected based on the results of the first phase of the study to be analyzed in more detail. Following a predesign using engineering methods, advanced computational methods are employed to refine and improve the design. This paper presents a synthesis of the comparison of predesigned VTVL and VTHL configurations as well as the current status of the in-depth analysis of one VTHL configuration selected after the study's first phase completion. The selection was done including aspects like development cost and risk, mission flexibility and system reliability.

The reference mission used for the predesign of various configurations consists of delivering 7.5 Mg to a geostationary transfer orbit (GTO) following a launch from Kourou. While the GTO mission serves as a baseline, performance for LEO, SSO and MEO is also assessed. The achieved payload masses are about 19 Mg for LEO, 15 Mg for SSO and 3 Mg for MEO.

2. STUDY BACKGROUND

The following parameters are considered important for obtaining comparable reusable first stages: thrust-to-weight ratio (T/W) at launch and upper stage delta velocity (ΔV). A T/W of 1.4 is used for all configurations analyzed in the frame of the study's first phase. The upper stage ΔV range of interest for VTVL stages has been narrowed down to a range of 6.6 to 7.0 km/s in [5] based on a preliminary analysis relying on empirical structural index functions. This has been further refined in [2] ruling out a ΔV of 6.6 km/s due to high reentry loads and descent propellant demand. Thus, for the presented work mainly upper stage ΔVs of 7.0 km/s are considered for VTVL. For VTHL no preliminary analysis based on structural index relations has been performed. Instead, a priori, hydrogen as fuel and staged combustion as engine cycle have been considered the best choice for the propulsion system because of the high achievable specific impulse. Therefore in case of VTHL some emphasis is placed on hydrogen staged combustion configurations and a range of upper stage ΔVs of 6.6, 7.0 and 7.6 km/s is considered. VTHL hydrogen, methane and kerosene gas generator configurations are designed for an upper stage ΔV of 7.0 km/s anticipating a comparison with VTVL configurations.

The necessary upper stage ΔV is considered to be a more precise way to compare different configurations than, for instance, reusable first stage separation Mach number, [5]. The above ΔV values refer to actual changes in velocity during powered flight. Another important aspect is the requirement of having the same fuel/oxidizer combination for the reusable first stages and the expendable upper stages. Also the same type of engine with different expansion ratios is used for the lower and upper stage. The number of stages is set to two for all analyzed configurations regardless of the propellant combination.

The reference target orbit parameters and launch site coordinates are:

- GTO 250 km × 35786 km, 6° inclination
- Kourou, French Guyana: 5.24° N / 52.77° W

The following return options are considered for reusable first stages:

- VTHL: Winged stage, Fly-Back (FB)
- VTHL: Winged stage, In-Air-Capturing (IAC)
- VTVL: Non-winged stage, Down Range Landing (DRL)

It should be noted that from an RLV stage performance point of view, IAC is to be considered equivalent to DRL. No analysis of the return flight of configurations consisting of the towing aircraft and the captured RLV stage is performed within this study. Current work on the IAC return method is described in [6].

3. DESIGN ASPECTS OF RLV CONFIGURATIONS

The basic architecture and geometry of the analyzed configurations is shown in Figure 1 on the example of three variants using LOX/LH2 as propellant combination. The VTVL configuration shown on the left (DRL) does have fins and landing legs as reusable first stage recovery hardware. In case of the two VTHL configurations shown in the middle (IAC) and on the right (FB), the reusable first stage is recovered by using a single delta wing and an aircraft-like landing gear.

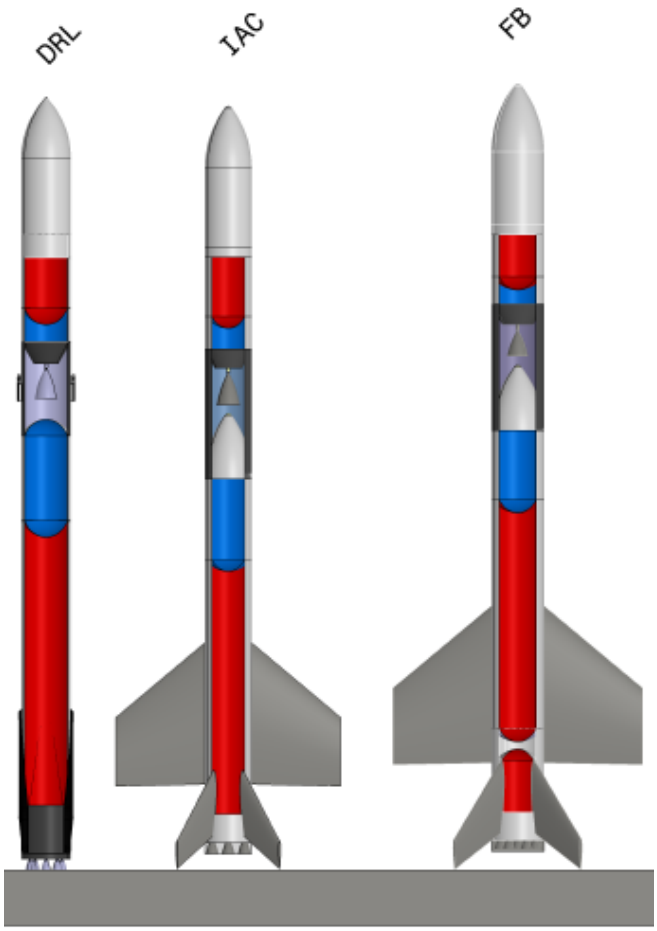

Figure 1: General architecture of analyzed configurations (LOX=blue, LH2=red)

Tandem staging is used for all configurations. The propellant tanks of the reusable first stage as well as the expendable upper stage are common bulkhead tanks. For both VTVL and VTHL an interstage structure is required between the lower and upper stages. Its length is influenced by the length of the upper stage engine and in case of VTHL also the first stage nose structure. Nose structure length is set to 7 m for all VTHL configurations. Upper stage engine expansion ratio is fixed to 120 for all studied variants.

In the following sections, two design aspects of major importance namely mass modelling and rocket propulsion subsystem analysis are described in more detail. Further details concerning the preliminary design of VTVL and VTHL configurations analyzed during the first phase of the presented study can be found in [1] and [3].

3.1. Mass Modelling

For the mass model a combination of empirical methods and preliminary structural analysis on the basis of selected load cases and structural concepts is used. The empirical mass estimation methods are based on stage loads, stage masses and geometrical parameters of the respective component. Structural analysis is performed using an in-house tool relying on beam theory. Masses of major structural elements as tanks, interstage structures and thrust frames are obtained by structural analysis whereas empirical

methods are applied for the majority of the remaining elements of the mass models. In particular the VTHL first stages wing is sized with empirical methods. The dimensioning parameters for the wing mass are lateral acceleration, stage dry mass, wing area, span and thickness. Load cases considered for structural analysis have been limited to ascent load cases and include the max q*alpha and launch pad load cases.

Tanks are modelled as stringer-frame stiffened common bulkhead tanks from aluminum alloy AA2219. Tank pressures are between 3 and 4 bars. Aerodynamic forces are computed with empirical methods. A safety factor of 1.25 is applied.

3.2. Rocket Propulsion

The two rocket engine cycles considered for the partly reusable configurations in this study are the Gas-Generator cycle (GG) and the Staged-Combustion cycle (SC). The thrust chamber pressure is set to 12 MPa for gas-generator engines. In the case of the staged combustion engines, the thrust chamber pressure is set to 16 MPa. Nozzle expansion ratios in the first stage are selected according to optimum performance but also requirements of safe throttled operations when landing VTVL stages. For the first stage of the VTVL configurations, the engine is computed for expansion ratios of 20 for gas generator types and 23 for the staged combustion variants. This value allows throttling, while still retaining sufficient nozzle exit pressure to prevent flow separation within the nozzle. A summary of VTVL engine parameters for the different propellant combinations and engine cycles is shown in Table 1.

Table 1: VTVL first stage rocket engine parameters

	LOX/RP-1	*LOX/LCH4*	*LOX/LH2*	
Cycle	**GG**	**GG**	**GG**	**SC**
MR [-]	2.25	2.5	6	6
SL Isp [s]	279	289	366	394
Vac. Isp [s]	310	320	406	428
T/W [-]	112	98	98	74

Since the VTHL configurations do not land vertically, the expansion ratio is set to 35 for both gas generator and staged combustion engines. A summary of VTHL configurations first stage rocket engine parameters is given in Table 2. The upper stage engines for both VTVL and VTHL are derived from the first stage engines, the only difference being the expansion ratio. In both cases its value is set to 120. This is considered to be a reasonable first assumption which takes into account length requirements of the interstage structure.

Table 2: VTHL first stage rocket engine parameters

	LOX/RP-1	*LOX/LCH4*	*LOX/LH2*	
Cycle	**GG**	**GG**	**GG**	**SC**
MR [-]	2.25	2.5	6	6
SL Isp [s]	267	276	351	386
Vac. Isp [s]	320	331	418	434
T/W [-]	113	99	96	72

All preliminary engine definitions have been performed by simulation of steady-state operation at 100% nominal thrust level using DLR in house tools as well as the commercial tool RPA (Rocket Propulsion Analysis). Any potential requirements specific to transient operations or deep-throttling are not considered in this early design study. Further, all engines considered in this study are designed with regeneratively cooled combustion chambers and regenerative or dump-cooling of the downstream nozzle extensions. Detailed information on the respective engine modelling is given in [2] and [7].

4. COMPARISON OF VTVL AND VTHL

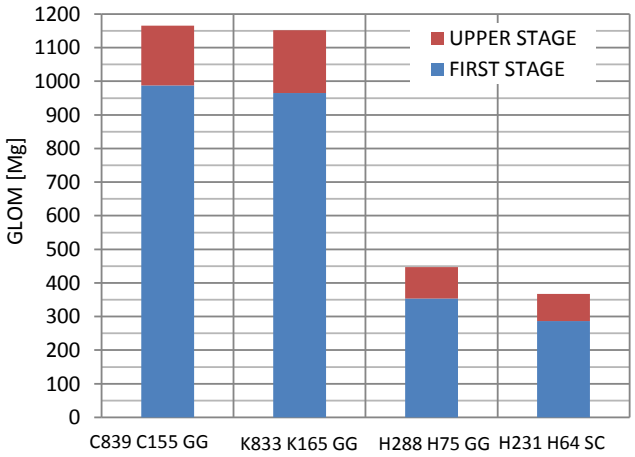

Figure 2: VTVL gross lift-off mass

To distinguish between the different configurations that are analyzed within the frame of this study the following nomenclature is used: after specifying whether the configuration is VTVL or VTHL the type of fuel (H=Liquid Hydrogen, C=Liquid Methane, K=RP-1), the ascent propellant mass in Mg and the rocket engine cycle (SC=Staged Combustion, GG=Gas Generator) are given. A configuration with a reusable first stage landing vertically, using methane as fuel, an ascent propellant loading of 839 Mg in the first and 155 Mg in the upper stage as well as gas generator rocket engines has e.g. the designation VTVL C839 C155 GG.

Gross lift-off masses (GLOM) of VTVL configurations are compared in Figure 2. It is showing the GLOM for systems with upper stage ΔVs of 7.0 km/s. For configurations using hydrogen, both gas generator as well as staged combustion cycles are considered. For methane and kerosene, only gas generator engines are used. All configurations shown in Figure 2 are down range landing systems. The large difference in GLOM between hydrocarbon and hydrogen systems is clearly visible. While for a design with hydrogen fueled staged combustion engines in both stages a GLOM of 367 Mg is achieved, the GLOM in case of hydrogen fueled gas generator engines increases to 447 Mg and in case of both methane and kerosene surpasses 1150 Mg.

Next Figure 3 shows lift-off masses of VTHL configurations with upper stage ΔVs of 7.0 km/s. Here, one of the configurations (FB) returns to the launch site by means of air-breathing propulsion, while the remaining ones are in-air captured. In case of the VTHL configurations the huge difference between hydrogen and hydrocarbons is also remarkable, but less pronounced than in case of VTVL. The lowest GLOM of 329 Mg

is achieved with hydrogen staged combustion engines and In-Air-Capturing as return method. Using gas generator engines and returning the reusable first stage to launch site by means of its own air-breathing propulsion system increases the GLOM to 385 and 443 Mg respectively. In case of methane and kerosene configurations GLOM is beyond 800 Mg.

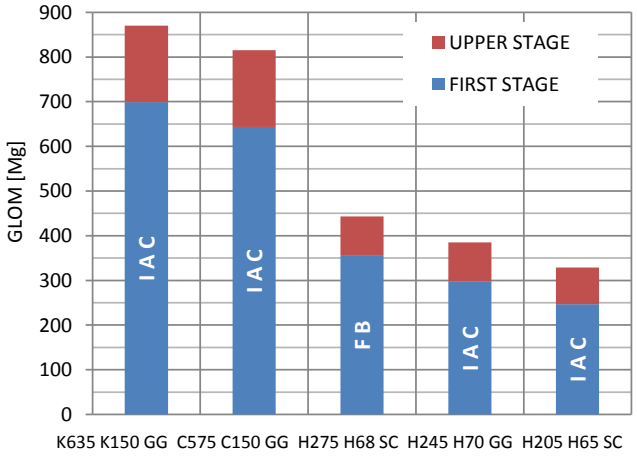

Figure 3: VTHL gross lift-off mass

Several aspects are of importance when discussing the GLOM results of the study's first phase. The GLOM of the entire configuration as well as the reusable booster stage is of course heavily influenced by the specific impulse of rocket engines. In case of VTHL hydrogen staged combustion engines, the vacuum Isp reaches 434 s whereas in case of kerosene, it decreases to 320 s, see Table 2. This huge loss of Isp of over 100 s has a negative impact on lift-off masses all by itself. When in a second step VTHL and VTVL are compared to each other, differences of first stage return methods also need to be considered. In contrast to VTHL, the VTVL rocket engines are used for both ascent and descent and obviously the ΔV generated by the first stage is higher. For the configurations shown in Figure 2 and Figure 3 the VTVL first stage ΔV is generally more than 1 km/s higher as compared to VTHL. As a consequence their sensitivity w.r.t. rocket engine efficiency must be higher as well. The effect of rocket engine efficiency on reusable first stage GLOM is shown in Figure 4 for VTVL and VTHL/IAC configurations with an upper stage ΔV of 7.0 km/s.

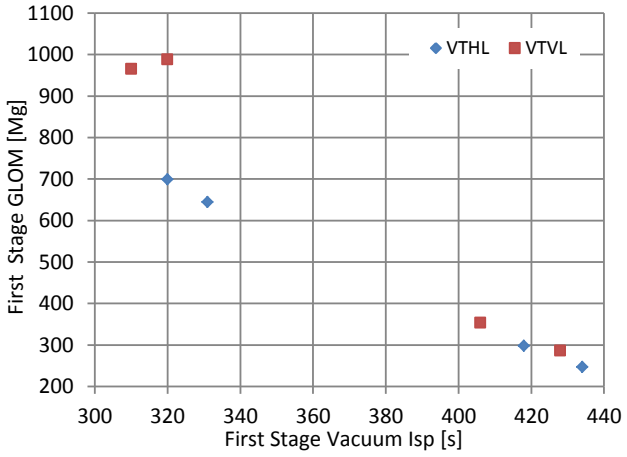

Figure 4: Effect of propulsion efficiency on first stage GLOM

While in case of hydrogen engines with vacuum Isp values of around 420 s the GLOM amplitude is about 100 Mg, it does increase to 350 Mg for kerosene and methane with vacuum Isp values of approximately 320 s. Another aspect contributing to the huge difference in GLOM between hydrogen and hydrocarbon configurations is related to launch vehicle staging. With the number of stages fixed to two for all analyzed configurations the remaining degree of freedom is the distribution of propellant between the reusable first stage and the expendable upper stage, which is equivalent to first stage separation velocity or upper stage ΔV. While the comparison of RLV stages having the same separation velocities leads to a more objective comparison in terms of e.g. reentry loads it does not take into account possible deviations from the theoretical optimal separation velocity that would lead to a minimum in total configuration GLOM or a maximum in payload fraction.

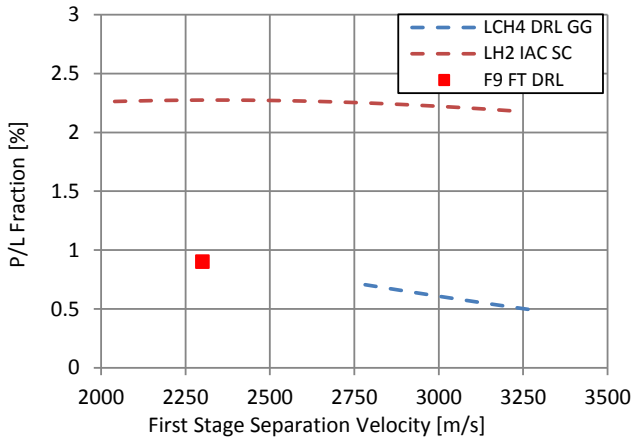

Figure 5: P/L fraction over first stage separation velocity

Based on mass and trajectory data obtained for the analyzed configurations it is possible to extract a relationship for the ratio of first stage ascent propellant w.r.t. total configuration engine cut-off mass (before first stage separation). This relationship can be in turn used to obtain the configuration GLOM and payload mass fraction as a function of first stage separation velocity via the rocket equation. Figure 5 shows the evolution of payload fraction over first stage separation velocity for a VTVL methane down range landing configuration using gas generator engines as well as for a VTHL In-Air-Capturing configuration using hydrogen staged combustion engines. The payload fraction trend in case of VTHL with hydrogen is relatively flat with a maximum close to 2800 m/s, which corresponds roughly to a first stage separation Mach number of 9. In contrast, for VTVL with methane as fuel, the trend is rather steep and not in proximity of the payload fraction maximum. Thus, an additional penalty is imposed on the hydrocarbon configurations by the chosen staging. Additionally, the payload fraction for the operational Falcon 9 launcher of SpaceX is shown. This data point is based on a DLR-SART recalculation of the SES-10 GTO mission of the Falcon 9 "Full Thrust" (FT) performing a down range landing of the first stage, [8]. At a first stage separation velocity of 2300 m/s a payload fraction of 0.9% is achieved by the launcher using LOX/RP-1 for both first and upper stage.

With the T/W ratio fixed to 1.4 for all analyzed systems the GLOM of the configuration is directly proportional to the required thrust at lift-off. Increased rocket engine thrust goes

together with an increase in rocket engine mass. In case of hydrocarbon configurations with high lift-off masses, this leads to an increased ratio of rocket engine mass w.r.t. the total stage dry mass. Knowing that a significant amount of stage cost is connected to its propulsion system this is of special interest in case dry mass is used as a figure of merit for RLV stage comparison.

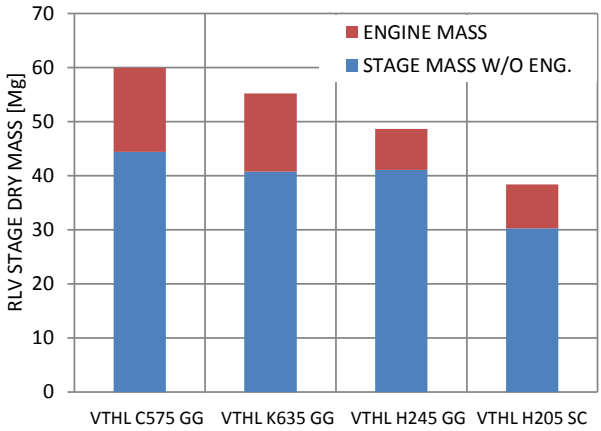

Figure 6: RLV stage dry mass for VTHL configurations

The reusable first stage dry mass for VTHL configurations with an upper stage ΔV of 7.0 km/s is shown in Figure 6. The dry mass of the methane stage reaches almost 60 Mg while in case of hydrogen staged combustion the dry mass is 38 Mg only. The rocket engine mass fraction is 26 % for methane and kerosene. For hydrogen gas generator engines it is 16 %, whereas it increases to 21 % for hydrogen staged combustion engines.

5. SELECTED VTHL CONFIGURATION

Based on the results of the first phase of the study the In-Air-Capturing configuration using hydrogen gas generator engines with a separation Mach number close to 9 was selected for further investigation. On the one hand, LOX/LH2 as propellant combination has the lowest masses for both VTVL and VTHL, on the other hand, it is believed that in Europe the development effort for a winged RLV stage relying on hydrogen gas generator engines will be smaller than in case of staged combustion engines. In the following, the current status and some specific design aspects of this VTHL system are presented. With respect to the first phase of the study, several aspects of the design are subject to changes. These are mainly related to structural analysis and include e.g. the use of a Kourou wind profile for structural load determination. Furthermore, the launch pad load case for fully loaded but unpressurized propellant tanks is added. Moreover, elements connecting the structural members are now considered and lead to an increase in structural mass. One major change compared to the first phase of the study is the more detailed definition of wing planform and size for the reusable first stage. The analysis starts with a predesign based on engineering methods similar to the first phase of the study. This predesign will be subsequently refined by inclusion of advanced computational methods and a higher level of detail in the fields of aerodynamics, aerothermodynamics, structural analysis and thermal protection system design.

5.1. General Architecture and Layout

The predesign of the configuration with a fixed-wing reusable first stage, an expendable upper stage and using hydrogen gas generator engines led to an overall GLOM of 385 Mg with a payload performance of 7.5 Mg to GTO.

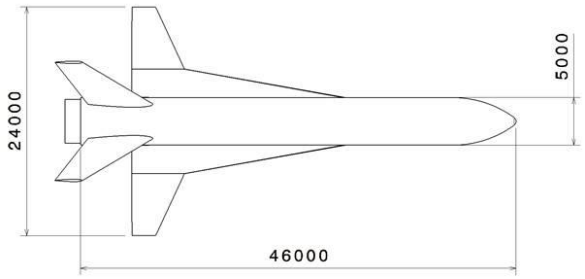

Figure 7: Reusable first stage geometry (H245)

The diameter of both the reusable first stage as well as the expendable upper stage is 5 m. Ascent propellant loading of the first stage is 245 Mg whereas the upper stage carries 70 Mg of liquid hydrogen and oxygen. The basic geometrical parameters of the resulting double delta wing first stage are shown in Figure 7. The total wing span is 24 m while stage length (without body flap) is 46 m. A body flap and trailing edge wing flaps are used for trimming. A NACA1408 airfoil is used at the root while an RAE2822 foil is used for the outer wing segment.

The gas generator engines of the first stage achieve a sea-level Isp of 356 s and a vacuum Isp of 416 s. The engine expansion ratio is 31. A sensitivity analysis of payload performance w.r.t. first stage engine expansion ratio does not show significant advantages in comparison to the expansion ratio value of 35 selected during the first phase of the study. But with a value of approximately 0.4 bar, the nozzle exit pressure of the gas generator engine with an expansion ratio of 31 is now equivalent to the one of the staged combustion engine with an expansion ratio of 35. This adaptation of engine expansion ratio better reflects the differences in engine cycle and thrust chamber pressure as compared to the first phase of the study where GG and SC engines had the same expansion ratio of 35.

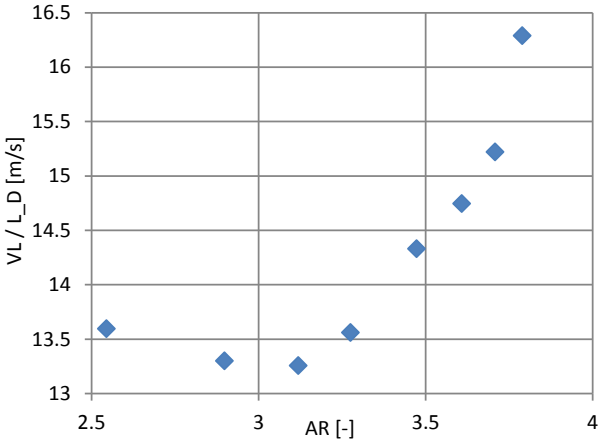

Figure 8: Variation of wing planform

The preceding variation of wing planform and area is carried out to a large extent from a subsonic aerodynamics point of view. The parameters considered to be design drivers are subsonic, trimmed lift-to-drag ratio and landing speed. To visualize the performed wing shape variation the ratio of landing speed to maximum, trimmed, subsonic glide ratio over wing aspect ratio is shown in Figure 8. The objective is to achieve sufficiently high subsonic lift-to-drag ratios and to not violate a defined landing speed limit. The trimmed, subsonic glide ratio is required to be higher than 6, whereas the landing speed limit is 100 m/s. The general wing planform is decided to be a double-delta. While the wing span value is maintained equal as compared to the corresponding design of the study's first phase, the inner segment leading edge sweep angle is varied from 25° to 80°. The outer segment leading edge sweep angle and wing tip chord length are kept constant at 25° and 2.7 m. The mid-chord length is 5.9 m. Variation of the inner wing segment leading edge sweep angle causes changes of wing area and wing aspect ratio. Glide ratio is evaluated at a Mach number of 0.4. Landing speed is calculated as stall speed multiplied with a factor of 1.3. The stage mass used for stall speed calculation consists of the stage mass without wing of 41.3 Mg and the varying wing mass, which is estimated using empirical methods. The maximum lift coefficient is taken at the upper end of the linear C_L range and a landing Mach number of 0.2. A minimum of the ratio of landing speed to glide ratio is found to be around an aspect ratio of 3. However, absolute wing area is of importance for trimming as well as the thermal loads experienced during the hypersonic part of the reentry trajectory. Therefore, the selected wing planform corresponds to the point with the minimum aspect ratio of 2.5 in Figure 8. The wing area is 140 m² while inner wing segment leading edge sweep is 80°.

5.2. Trajectory

Ascent trajectory optimization is performed with a direct method and uses Sequential Quadratic Programming (SQP). The payload mass delivered to orbit is the optimization objective while pitch rate and thrust angle (w.r.t. velocity) are used as controls. Axial acceleration is limited to 50 m/s². In contrast to the ascent trajectory, the descent trajectory is the result of a simulation taking into account thresholds for mechanical and thermal loads like dynamic pressure, stagnation point heat flux and normal acceleration. It serves as a reference for the more detailed analysis of aerodynamics, aerothermodynamics and thermal protection system design. The descent trajectory is shown in Figure 9. From the point of reusable first stage separation at an altitude of 62 km and a Mach number of 8.9 the altitude increases to its maximum value of 92 km prior to atmospheric reentry. The empirically estimated nose stagnation point heat flux reaches a peak value of 179 kW/m² at an altitude of 37.6 km and a Mach number of 6.8. The first stage nose radius is 0.5 m and a cold wall is assumed. Maximum values of 20 kPa and 3.2 g are reached for the dynamic pressure and normal acceleration respectively. At about 50 km altitude a banking maneuver is initiated to reorient the trajectory heading towards the launch site. A maximum banking angle of 40° is allowed. The orthodrome distance to the launch site after reentry and turn is 950 km.

For the ascent trajectory of the H245 H70 configuration it is important to note that due to the requirement that the line of apsides of the GTO ellipse has to be in the equatorial plane, upper stage flight is split into two thrust phases with a ballistic phase in between. Thus, the initial part of the ascent consists of the first stage thrust phase plus the first thrust phase of the upper stage and allows reaching an intermediate orbit that is followed until crossing the equator. Above the equator, the upper stage is reignited and apogee reaches GEO altitude. The intermediate orbit has a perigee altitude of 140 km, an apogee altitude of 330 km and an inclination of 5.9°. At the end of the ascent a velocity of 9.7 km/s is reached. Along the ascent trajectory a maximum dynamic pressure of 38 kPa and a peak stagnation point heat flux of 91 kW/m² are reached. Total gravity losses sum up to 1224 m/s, while drag and thrust losses are 147 m/s and 46 m/s respectively.

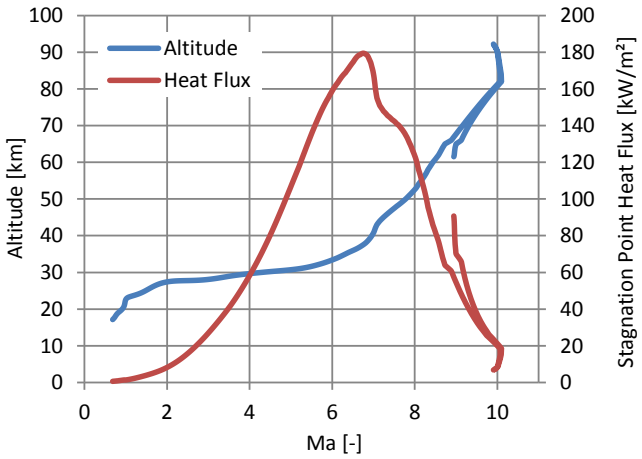

Figure 9: H245 reusable first stage reentry trajectory

5.3. Aerodynamics

In the frame of the predesign based on engineering methods, ascent aerodynamics is modelled with empirical methods for simple fuselage wing combinations. Lift, drag and pitch moment coefficients as a function of angle of attack and Mach number in the subsonic, supersonic and hypersonic regimes are calculated. Methods for fuselage aerodynamics are based on slender body theory. Wing aerodynamics is based on empirical lifting line methods. Descent aerodynamics is analyzed with the same empirical methods in subsonic as well as supersonic regimes and with a surface inclination tool in the hypersonic regime.

To improve the descent trajectory analysis, a comprehensive aerodynamic database for the entire Mach number range is generated using DLR´s TAU code. Aerodynamic coefficients are obtained by solving the inviscid Euler equations, utilizing a second order upwind flux discretization scheme together with a backward Euler relaxation solver. As a result of mesh sensitivity analysis an unstructured mesh with 820 10³ nodes was chosen as a trade-off between solution accuracy and calculation time. The calculation points are extracted from a reference trajectory with Mach number ranging from 0.5 to 9. The angle of attack values range from -10° up to +45°. The pressure coefficient distribution for a subsonic flight point is shown in Figure 10. The pressure distribution shown is for a subsonic cruise flight point in 5 km altitude at a Mach number of 0.5. The angle of attack is 5°. The area of low pressure coefficient at the outer wing leading edge is clearly visible. This constitutes a potential problem concerning the choice of airfoil section for the outer wing segment. In the frame of the configuration predesign, the RAE2822 airfoil has been selected, as described in section 5.1. Due to the airfoil

geometry, in particular the small airfoil nose radius and the rather high angle of attack for subsonic cruise flight, the flow acceleration on the upper airfoil surface in the vicinity of the leading edge is very strong. This has the potential to make the flow partially supersonic which is also shown by RANS calculations. Thus, the choice of airfoil section will be reassessed during subsequent design iterations.

Calculations are performed with three different geometries having negative, neutral and positive flap deflection angles. The maximum allowed absolute flap deflection magnitude is 20°. The body flap is allowed to have positive deflection angles only (downward deflection). Interim values of the aerodynamic coefficients are linearly interpolated within the mentioned extrema and zero positions. The descent aerodynamic database consists of 140 calculations for each flaps setting. The validation of the Euler results is done by RANS calculations for specific flight points. For the ascent configuration the influence of running rocket engines and their exhaust gas jets on aerodynamic drag is analyzed by a two gas simulation. For the rocket engine exhaust gas properties average values corresponding to the respective combustion products are used. The ascent calculations feature no flap deflection. For the reference ascent trajectory 90 calculations are performed.

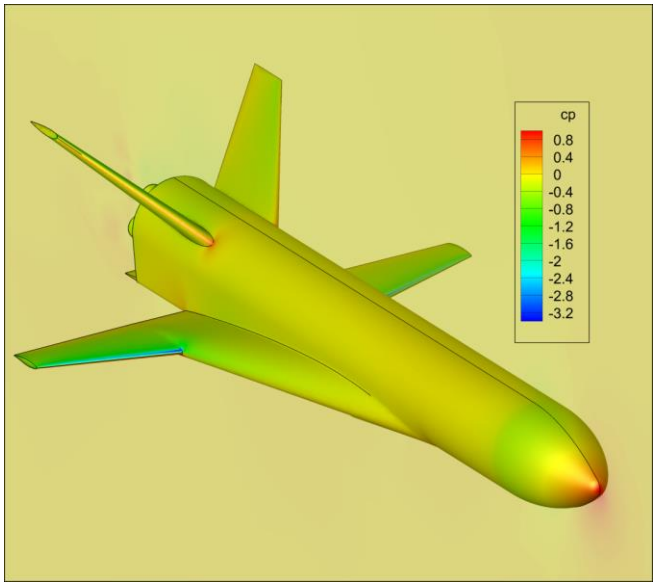

Figure 10: Pressure coefficient distribution H245 stage (Mach=0.5, Altitude=5 km, AoA=5.0°)

5.4. Aerothermodynamics

To assess the aerothermodynamic heating during atmospheric reentry and to prepare detailed thermal protection system design, an aerothermodynamic database (AETDB) is created based on eleven trajectory points of the reference descent trajectory. The heating predictions are based on viscous simulations with fully resolved boundary layers. Turbulence is modelled using a one-equation RANS approach. Thermodynamics is treated with an equilibrium gas model which includes high temperature effects such as vibrational excitation of the molecules and chemical dissociation. Four initial wall temperatures from 200 to 1100 K are considered. An exemplary heat flux distribution for the peak heating flight point is shown in Figure 11. In the area of the nose a heat flux of around 200 kW/m² is reached.

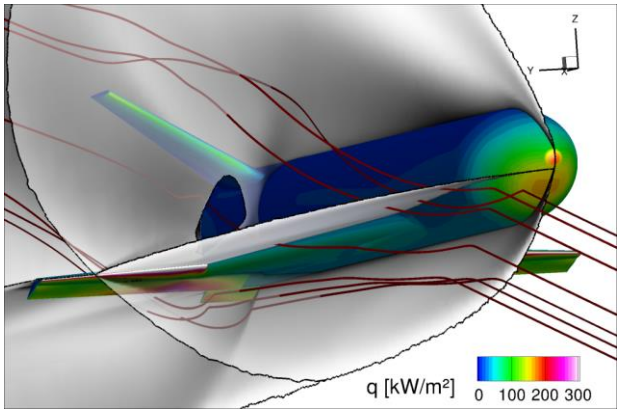

Figure 11: Heat flux distribution for the peak heating flight point (Mach = 6.8, Altitude = 37.6 km, AoA=12°)

The entirety of the obtained heat flux data is organized in a data base, which, together with appropriate interpolation algorithms, forms a complete surrogate model for the aerothermal heating of the vehicle. The local heat flux distribution can be obtained for any flight time and any surface temperature distribution. This surrogate model can be easily coupled to transient structural analysis tools to calculate local surface temperature evolutions during the reentry flight. Results in form of a temperature distribution are shown in Figure 12. The structural heating response was treated with a simple lumped-mass model. The initial surface temperature at t=0 s was assumed to be 200 K. The results in Figure 12 show the maximum surface temperatures, which occur at an altitude of around 30 km and a Mach number of approximately 4.4. It should be noted that this flight point is different from the point of maximum nose stagnation point heat flux at an altitude of 37.6 km. Critical components of the vehicle are the control surfaces, the leading edges of the outer wings and rudders as well as the vehicle nose.

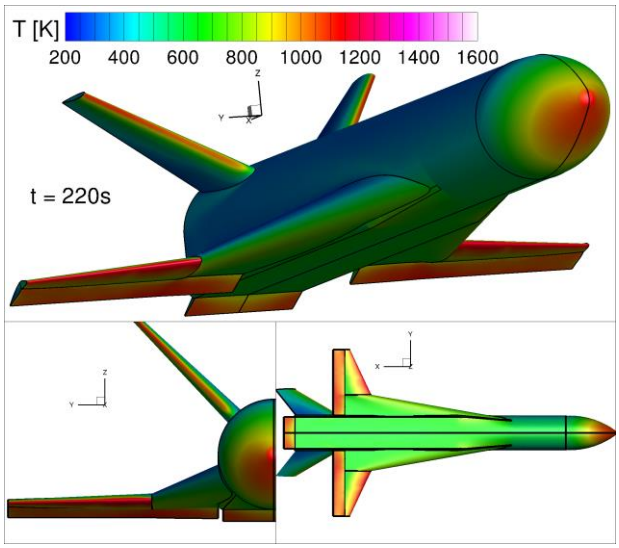

Figure 12: Temperature distribution resulting from a simple lumped-mass model (Mach=4.4, Altitude=30 km)

6. CONCLUSIONS AND OUTLOOK

In this paper a selection of partially reusable, two-stage, VTVL and VTHL launch vehicle configurations is compared and the current status of the analysis for one selected VTHL configuration is presented. For all analyzed configurations a payload performance target of 7.5 Mg to GTO is set. Performance for other target orbits is also assessed. Comparison of VTVL and VTHL in terms of GLOM and dry mass is presented. In case of the VTHL configuration selected based on the results of the study's first phase, the focus is on the architecture of the winged reusable first stage as well as on current, ongoing work in the area of aerodynamics and aerothermodynamics.

In the frame of the comparison of VTVL and VTHL configurations, two aspects are of major importance when summarizing the results of the first phase of the study. On the one hand, it is the pure choice of the propellant combination and rocket engine cycle regardless of the particular first stage return option. On the other hand, the comparison of the VTVL and VTHL configurations including their specific first stage return methods can be considered. Concerning the choice of the propellant combination the highest gross lift-off masses are obtained with the configurations using methane and kerosene. The same is true when comparing the dry mass of the reusable first stages. In contrast, configurations relying on LH2 as fuel and staged combustion as engine cycle do have the lowest GLOM and dry mass values. The ratio of first stage rocket engine mass to the first stage dry mass, the rocket engine mass fraction, is as well highest for hydrocarbon configurations whereas LH2 gas generator configurations have the lowest engine mass fractions. However, when comparing different propellant combinations in use on configurations with similar upper stage ΔVs, it should be noted that the points of optimum staging are not the same. Regarding the comparison of VTVL and VTHL configurations a general significant advantage of one over the other is not found based on the results of the performed analysis. In case highly efficient rocket propulsion systems are employed, lift-off as well as dry masses are very close to each other. However, it is very important to note, that the sensitivity w.r.t. rocket engine efficiency is clearly higher for VTVL configurations than for their VTHL counterparts.

Two conclusions can be drawn based on the above results synthesis. First, it can be concluded that the use of hydrogen staged combustion propulsion is beneficial regardless of whether a VTVL or a VTHL approach is followed. Second, although the chosen staging does impose a certain penalty on hydrocarbon configurations, they do not seem to be promising looking at the comparison of total configuration lift-off mass, reusable first stage dry mass and rocket engine mass fraction. This is especially true for VTVL hydrocarbon configurations due to their increased sensitivity to rocket engine specific impulse. Furthermore, it could be argued that if the decision to select a propellant combination with a lower Isp is taken, a VTHL approach would be more suitable due to its reduced sensitivity w.r.t. the propulsion efficiency. On the other hand, a higher sensitivity of VTVL configurations to propulsion efficiency would allow them to benefit more from a possible enhancement of rocket engine efficiency.

The current status of the ongoing analysis of the H245 H70 GG configuration, which has an overall lift-off mass of 385 Mg, is shown. The reusable first stage predesign features a double-delta wing resulting from a trade-off between subsonic glide ratio and landing speed. Advanced computational methods in the area of aerodynamics and aerothermodynamics are employed to support subsequent design iterations. The next foreseen steps include adaptations to the reusable first stage geometry and a refined trim analysis based on the created aerodynamic database. The definition and design of the thermal protection system will be improved using the presented aerothermodynamic database.

7. ACKNOWLEDGEMENTS

The authors would like to acknowledge the contribution of everyone involved in the XTRAS/ENTRAIN system study and the design process of the presented partially reusable launcher configurations.

8. REFERENCES

1. J.Wilken, S. Stappert, L. Bussler, M. Sippel, E. Dumont, "Future European Reusable Booster Stages: Evaluation of VTHL and VTVL Return Methods", *69th IAC*, Bremen 2018

2. S. Stappert, J. Wilken, M. Sippel, E. Dumont, "Assessment of a European Reusable VTVL Booster Stage", *Space Propulsion Conference*, Seville 2018

3. L. Bussler, J. Wilken, S. Stappert, M. Sippel, I. Dietlein, E. Dumont, „Assessment of VTVL and VTHL Reusable First Stages", *HiSST Conference*, Moscow 2018

4. M. Sippel, L. Bussler, S. Krause, S. Cain, S. Stappert, „Bringing Highly Efficient RLV-Return Mode In-Air-Capturing to Reality", *HiSST Conference*, Moscow 2018

5. E. Dumont, S. Stappert, T. Ecker, J. Wilken, S. Karl, S. Krummen, M. Sippel, "Evaluation of Future Ariane Reusable VTOL Booster Stages", IAC-17-D2.4.3, 68th *International Astronautical Congress*, Adelaide 2017

6. M. Sippel, S. Stappert, L. Bussler, S. Krause, S. Cain, J. Espuch, S. Buckingham, V. Penev, "Highly Efficient RLV-Return Mode "In-Air-Capturing" Progressing by Preparation of Subscale Flight Tests", *8th EUCASS Conference*, Madrid 2019

7. M. Sippel, J. Wilken, "Preliminary Component Definition of Reusable Staged-Combustion Rocket Engine", *Space Propulsion Conference*, Seville 2018

8. S. Stappert, M. Sippel, "Critical Analysis of SpaceX Falcon 9 v1.2 Launcher and Missions", SART TN-009/2017